Journal of Aerosol Science 54 (2012) 77–87

Contents lists available at SciVerse ScienceDirect

Journal of Aerosol Science

journal homepage: www.elsevier.com/locate/jaerosci

Effects of gas species on pressure dependence of thermophoretic velocity

Bin Razali Mohd Azahari [a,b,*], Masayuki Mori [a], Masataro Suzuki [a], Wataru Masuda [a]

[a] Nagaoka University of Technology, 1603-1 Kamitomioka, Nagaoka, Niigata 940-2188, Japan
[b] University Tun Hussein Onn Malaysia, Parit Raja, Batu Pahat, 86400 Johor, Malaysia

ARTICLE INFO

Article history:
Received 24 April 2012
Received in revised form
29 June 2012
Accepted 1 July 2012
Available online 9 July 2012

Keywords:
Microgravity experiment
Thermophoretic velocity
Tangential momentum accommodation coefficient
Thermal accommodation coefficient

ABSTRACT

Microgravity experiments are conducted to measure the thermophoretic velocity, and effects of gas species are investigated. Particles adopted are PMMA spheres of 2.91 μm in mean diameter, and atmospheric gases chosen are pure gases of argon, nitrogen, and carbon dioxide. The temperature gradient is set at 10 K/mm, and the pressure is set at several conditions in the range from 20 kPa to 100 kPa. Terminal velocities of particles suspended in a gas are individually measured during 0.25 s of the microgravity condition, which is achieved by a free-fall. The accuracy of the measurement is attained by accumulating data from repeated trials. Obtained experimental results are compared with theoretical predictions; a notable discrepancy is found for carbon dioxide, while the results for other two gases are consistent with predictions. Some attempts are made to fix the discrepancy: first by modifying constants and second by modifying two empirical coefficients in the theory.

1. Introduction

Thermophoresis is the phenomenon that a small particle in a gas with a temperature gradient moves toward the lower temperature side. This phenomenon is supposed to influence practically on the movement of soot particles in exhaust gas from combustors, especially near cool walls around the hot gas flow, where the temperature gradient can become as large as the order of 10^2 K/mm. For example, the measured size-distribution of particulate matter is influenced by the temperature of the transfer tube connecting the exhaust pipe of a diesel engine to the dilution tunnel ahead of the measuring device (Yuasa et al., 2011). A soot particle is generally an aggregate of fine primary spheres. There have been some direct measurements on the thermophoretic phenomenon of such an aggregate particle. Zheng & Davis (2001) have measured the thermophoretic force acting on an aggregate of polystyrene latex spheres, and found that the force is affected by the number of primary spheres in the aggregate. Dobashi et al. (2000) and Suzuki & Dobashi (2007) have conducted direct measurements on the thermophoretic velocity of soot particles, and have revealed that the velocity is dependent not only on the macroscopic size of the soot particle but also on the aggregating condition; Suzuki & Dobashi (2007) have shown experimental results suggesting that the phenomenon is dominated by the size of primary spheres when the aggregation is coarse. Thus, the understanding of the phenomenon for a single sphere is indispensable before understanding for an aggregate.

* Corresponding author at: Masuda Suzuki Laboratory, 2nd Floor, Mechanical Building, Nagaoka University of Technology, 1603-1 Kamitomioka, Nagaoka, Niigata 940-2188, Japan. Tel.: +81 80 4298 2710.
E-mail addresses: azahari@uthm.edu.my, m-azahari@msl.nagaokaut.ac.jp (B.R. Mohd Azahari).

0021-8502/$ - see front matter © 2012 Elsevier Ltd. All rights reserved.
http://dx.doi.org/10.1016/j.jaerosci.2012.07.002

The thermophoretic phenomenon of a spherical particle has been studied both theoretically and experimentally. Theoretical works have been carried out by considering the boundary condition on the surface of a single spherical particle suspended in a gas with a temperature gradient. Brock (1962) derived a theoretical solution to the thermophoretic force on the particle by applying a slip boundary condition on its surface, which includes effects of the thermal slip, the viscous slip, and the temperature jump. Derjaguin & Yalamov (1965) derived the thermophoretic velocity from the Brock's theoretical solution by equating the balance between the thermophoretic and the drag forces.

Experiments, on the other hand, have been performed by measuring the thermophoretic force or the thermophoretic velocity. Fredlund (1938) attempted a systematic experiment to examine the effect of the temperature field upon a disk suspended on a balance. The thermophoretic force and the thermophoretic velocity are measured by several methods: Millikan cell (Rosenblatt & La Mer, 1946; Saxton & Ranz, 1952; Schadt & Cadle, 1961; Jacobsen & Brock, 1965), electrodynamic balance (Li & Davis, 1995a, 1995b), precipitation in a thermoprecipitator (Schadt & Cadle, 1957; Keng & Orr, 1966), jet technique (Kousaka et al., 1976; Prodi et al., 1979; Talbot et al., 1980), and deflection of a particle suspended by a small wire (Davis & Adair, 1975; Tong, 1975).

Above experimental methods are complex in practical implementation, and as a consequence, involve numerous errors. Among those, errors caused by buoyancy are the largest problem; in a field with a temperature gradient, buoyancy induces natural convection, which influences the movement of particles and disturbs the measurement. The velocity of such natural convection is usually comparable to the thermophoretic velocity, and cannot be measured directly. To avoid this problem, some experiments have been conducted under microgravity conditions. Toda et al. (1996, 1998) performed experiments in a drop tower facility and demonstrated that the microgravity environment satisfactorily suppresses the disturbance. Prodi et al. (2006, 2007) also conducted microgravity experiments by means of a drop tower facility and/or parabolic flights. However, their reported data still seem to contain errors, possibly owing to limited trial numbers of experiments, so that those data are not sufficient to make quantitative comparison with theories (Suzuki et al., 2009a).

Recently, our group has developed a device for conducting experiments repeatedly under a microgravity environment in a very short period time, i.e. 0.3 s, by means of the free-fall method, to accumulate data of the thermophoretic velocity. It has been confirmed that satisfactory accuracy can be attained if the amount of data is sufficient for statistical treatment (Suzuki et al., 2009a). By comparing the obtained experimental results with the existing theory (Brock, 1962), two notable differences are found; one is the substantial difference for particles with high thermal conductivity, and the other the remarkable difference in the dependence of the humidity in the air (Suzuki et al., 2009b). The problem of the former difference has been solved by reconsidering the boundary condition to improve the theory (Hoshino et al., 2010a). Hoshino et al., (2010b) has derived an improved theoretical solution of the thermophoretic velocity by applying the boundary condition proposed by Lockerby et al. (2004), which includes the thermal stress slip and the higher order isothermal slip. However, even this improved theory cannot solve the problem of the latter difference. The deviation of the theory from the experiment infers that the composition of the surrounding gas mixture has some unknown influence on the phenomenon.

Before analyzing the influence of the composition of the gas mixture, it is indispensable to know the characteristics of the phenomenon for each gas component. Thus, in this study, the characteristics of the thermophoresis for several gas species, i.e., argon, nitrogen, and carbon dioxide are experimentally examined. The first one is chosen as the reference, and the latter two are chosen as the major components of exhaust gas from combustors. Water vapor is the clue of starting this work, but it is excluded owing to technical reasons on conducting the experiment.

2. Theory for thermophoretic velocity

The theory adopted in this work is based on the works by Hoshino et al. (2010b) and by Chang & Keh (2012). The thermophoretic velocity is calculated from the balance between the thermophoretic and the drag forces, the equation of which is shown as below

$$V_T = \frac{2\mu C_f}{\rho T_{F0}} \frac{[C_S(k+C_T Kn)+C_H(C_M C_T Kn^2+C_M Kn[k-1])]}{[1+3C_M Kn+h](1+2k+2C_T Kn)} |\nabla T|, \tag{1}$$

where μ, $|\nabla T|$, ρ, T_{F0}, C_f, k, Kn, h, C_M, C_T, C_S, and C_H are the viscosity, the temperature gradient, the density of the surrounding gas, the reference temperature, the slip correction factor of the drag force for rarefied condition, the gas-to-particle thermal conductivity ratio, Knudsen number, the term of higher order isothermal slip, and constants for slip flow, temperature jump, thermal creep, and thermal stress slip, respectively. Here, the reference temperature T_{F0} is defined as the supposed gas temperature at the center of the particle in the given temperature field without the existence of the particle, and Knudsen number Kn is the ratio of the mean-free-path l to the particle radius. The mean-free-path is calculated from the following equation (Kennard, 1938):

$$l = \frac{\mu}{0.499P}\sqrt{\frac{\pi R T_{F0}}{8}}, \tag{2}$$

where P and R are the pressure and the gas constant, respectively. The slip correction factor C_f adopted in this work is Cunningham's correction factor $C_{fc} = 1 + A\,Kn$, where $A = 1.257 + 0.4\exp(-1.10/Kn)$ (Talbot et al., 1980). The term h of

higher order isothermal slip is written as below

$$h = \frac{9}{2\pi}\mathrm{Pr}Kn^2(1-\gamma^{-1}) \tag{3}$$

where Pr and γ are Prandtl number and the specific heat ratio, respectively.

Eq. (1) is basically identical to both of those proposed by Hoshino et al. (2010b) and Chang & Keh (2012). If constant values $C_S=0.75$ and $C_H=1.00$ (Lockerby et al., 2004) are applied, the equation becomes just the same as the one given by Hoshino et al. (2010b). On the other hand, the equation becomes the same as the one given by Chang & Keh (2012) by neglecting the term h, which is usually negligible in the range of $Kn \le 0.1$, and applying Basset's correction (Basset, 1961), $C_{fb} = (1+3C_MKn)/(1+2C_MKn)$, instead of the Cunningham's correction for the slip correction factor C_f. The Basset's correction is applicable in $Kn \le 0.1$ while the Cunningham's one in $Kn < 1$, and both are basically identical in those applicable ranges.

Two constants C_M and C_T are calculated as follows from two empirical coefficients, i.e., the tangential momentum accommodation coefficient α_m and the thermal accommodation coefficient α_t

$$C_M = \frac{2-\alpha_m}{\alpha_m}, \tag{4}$$

$$C_T = \frac{15}{8}\left(\frac{2-\alpha_t}{\alpha_t}\right). \tag{5}$$

These accommodation coefficients represent the magnitude of the momentum and energy exchange in the collision between gas molecules and the particle (Kennard, 1938; Shen, 2010), which are defined as below

$$\alpha_m \equiv \frac{M_i-M_r}{M_i-M_s}, \tag{6}$$

$$\alpha_t \equiv \frac{E_i-E_r}{E_i-E_s}, \tag{7}$$

where M and E are average tangential components of the momentum and the energy flux normal to the particle surface, respectively, of gas molecules, and subscripts i, r, and s refer to incident molecules, molecules reflecting from the surface, and molecules leaving the surface in equalibrium with the surface, respectively. For example, $\alpha=1$ corresponds to the situation that incident molecules achieve complete equilibrium with the particle surface before leaving, while $\alpha=0$ corresponds to the situation of complete specular reflection.

In many cases, values of accommodation coefficients are simply assumed to be unity (Suzuki et al., 2009b; Hoshino et al., 2010a). There are some experimental measurements, e.g., Thomas & Lord (1974) and Douglas (1982), who measured accommodation coefficients on steel spheres and gas covered tungsten tube, respectively. Although those experiments report values different from unity under some conditions, yet there are no commonly accepted values.

3. Experimental

3.1. Apparatus

Fig. 1 shows a schematic of the apparatus, which includes a drop tower, a measuring unit, and a damping cushion. The measuring unit is hung at the top of the drop tower by an electric magnet. The unit starts falling when the electric

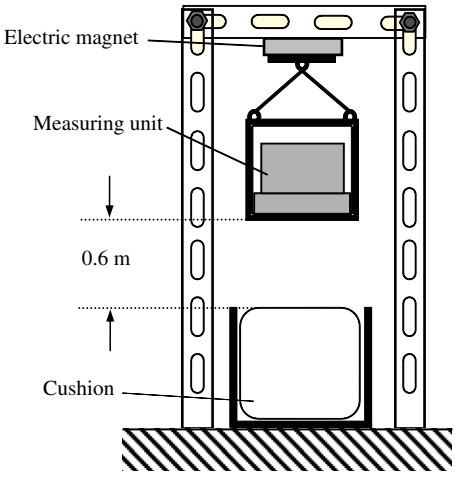

Fig. 1. Schematic of apparatus.

magnet is deactivated. The falling distance is 0.6 m, which corresponds to the duration time of the microgravity condition at 0.3 s.

Fig. 2 shows a variation of the gravity level during an experiment. The gravity level is measured by the G-sensor attached on the measuring unit. The duration time of the free-fall is about 0.3 s as seen in the figure. When the electric magnet is deactivated at $t=0$, the gravity level in z-axis changes from -1.0 G to $+0.4$ G once, possibly owing to the vibrational motion of the frame of the unit, and then decays as time passes until the unit reaches the cushion. The range between ± 0.1 G in gravity level is regarded as the microgravity condition in this work, the duration time of which is about 0.25 s.

Fig. 3 shows a cross-section of the pressure vessel, the main part of the measuring unit. Placed in the vessel is a cylindrical thin chamber of 1.5 mm in height between two opposing aluminum plates. The upper plate, initially at the room temperature, is kept cool by moving it 15 mm away from the bottom plate while the latter is under the process of heating to raise its temperature. Keeping this arrangement, the vessel is evacuated by a pump. When the bottom plate reaches the appointed temperature, the upper plate is put in place where the distance between the plates is 1.5 mm. Then, the vessel is filled with the test gas. When the temperature of the upper plate becomes the target temperature, both electromagnetic valves at the inlet and the outlet are simultaneously opened for 0.01 s such that some particles are blown into the chamber from a particle reservoir upstream the inlet. The magnet holding the measuring unit is deactivated 0.84 s after the closure of both valves. The disturbances caused by the blow are expected to cease within this period before the drop; since it is larger than both characteristic times for the flow field and the temperature field to reach the steady state; those characteristic times are expressed as $t_f=(\delta/2)^2/\nu$ and $t_t=(\delta/2)^2/\alpha$, respectively, where δ, ν, and α are the distance between two plates, the kinematic viscosity, and the thermal diffusivity, respectively (Toda et al., 1996,1998). The largest values of those for present conditions are estimated at 0.06 s and 0.05 s. Those blown particles are illuminated by the laser

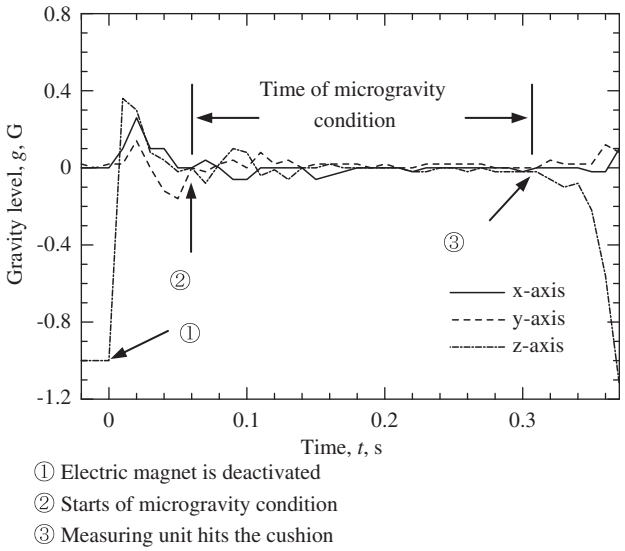

Fig. 2. Gravity level during experiment Gravity level is measured by the G-sensor which is attached on the measuring unit.

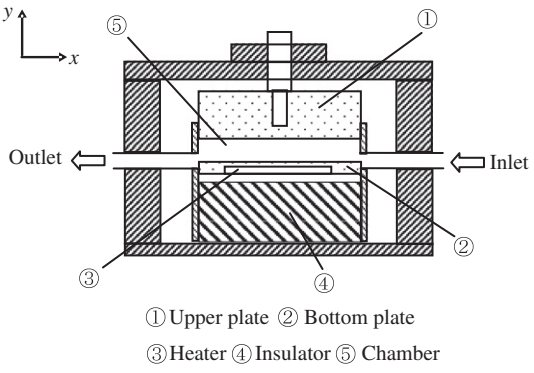

Fig. 3. Schematic of pressure vessel.

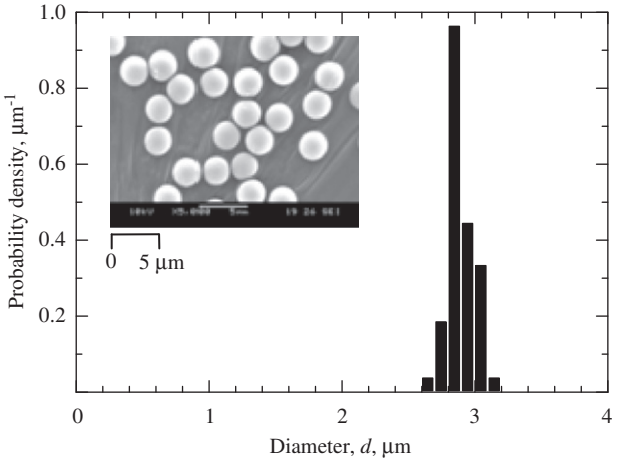

Fig. 4. Diameter distribution of particles.

beam introduced into the chamber to produce scattering lights, the image of which is recorded by a high-speed camera under the condition of the frame rate at 200 fps and of the shutter speed at 2 ms.

3.2. Sample particles and experimental condition

Sample particles used in this work are PMMA sphere particles from Sekisui Plastics Co., Ltd. These are chosen since the size is quite uniform; Fig. 4 shows the probability density distribution of the particle diameter d measured from SEM images. The mean diameter and the standard deviation are 2.91 μm and 0.09 μm, respectively. The thermal conductivity is measured by the manufacturer at 0.21 W/(mK).

Experiments are conducted under the microgravity condition with the test gas of argon, nitrogen or carbon dioxide. The target temperature and the temperature gradient are 313 K and 10 K/mm, respectively. The temperature field during the experiment is monitored by measuring temperatures at two points in the vessel: one is in the top plate and the other in the bottom one. The temperature field is controlled based on these measured temperatures. Before making experiments, the preparatory measurement for the temperature field is conducted by inserting two more thermocouples suspended in the chamber at different heights. Measuring two points is sufficient because the linearity of the temperature field has already been confirmed by the Mach–Zehnder interferometry (Toda et al., 1996,1998). The relation between these temperatures at monitoring points and the actual temperature field in the chamber is examined from this preparatory measurement. When conducting thermophoresis experiments, additional two thermocouples are removed; the temperature field is controlled based on the temperatures at those two monitoring points.

Various pressure conditions are chosen from 20 kPa to 100 kPa. The thermophoretic velocity for each particle is individually measured, and the mean value and the 95% confidence interval for each experimental condition are statistically obtained.

4. Results

Fig. 5 shows examples of the movement of particles during a free-fall in the surrounding gas of argon at 20 kPa. The measurement of the velocity should be taken at a fixed temperature since the thermophoretic velocity is dependent on not only the temperature gradient but also the temperature itself. The velocity of each particle is measured by tracing its movement while it travels within the range of the temperature between 313 ± 2 K. It is seen from the figure that the velocity of each particle can be considered as constant in the range. The velocity is constant also in other two gases.

Table 1 shows the statistical data for the tested pressure conditions with the argon gas. It is noted that the 95% confidence interval indicates not the range of data scattering but the range of expected mean value of the population. It is seen that the confidence interval is roughly estimated at around 0.01 mm/s to 0.02 mm/s. The ratio of the confidence interval to the mean value is only 3% for the pressure at 20 kPa. As the pressure increases, the velocity decreases, and as a consequence, the ratio tends to increase.

Fig. 6 shows the thermophoretic velocity for each gas. The white rectangle (□), the black circle (●), and the white circle (○) represent experimental values for argon, nitrogen, and carbon dioxide, respectively. Error bars in the figure indicate the 95% confidence interval. The solid line is the prediction calculated by assuming constants to be identical to those in the previous work (Hoshino et al., 2010a), namely, C_M, C_T, C_S, and C_H to be 1.000, 1.875, 0.750, and 1.000, respectively.

For argon and nitrogen, predictions are in good agreement with experiments throughout all the tested pressure conditions; the solid line runs through the range of the confidence interval at every tested pressure. On the other hand, for carbon dioxide, discrepancy is seen at low pressure conditions; the prediction is within the range of the confidence interval

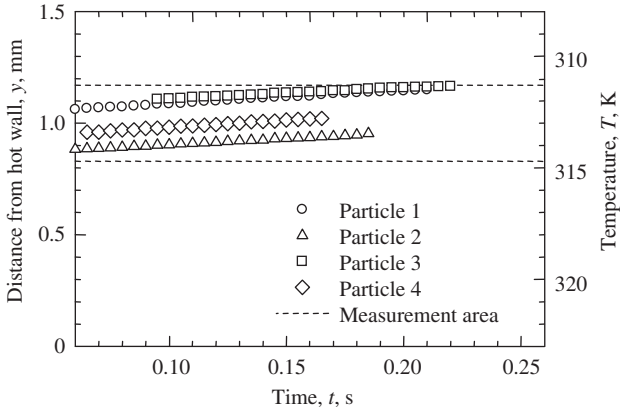

Fig. 5. Movement of particles in surrounding gas of argon.

Table 1
Statistical data of thermophoretic velocity in surrounding gas of argon.

Pressure, P, kPa	20	40	60	80	100
Sampling number, n, –	39	35	37	33	47
Mean thermophoretic velocity, $\overline{V_T}$, mm/s	0.538	0.183	0.111	0.075	0.066
Standard deviation, σ, mm/s	0.053	0.044	0.026	0.030	0.036
Confidence interval (95%), mm/s	0.017	0.015	0.009	0.011	0.011
Ratio of confidence interval to mean thermophoretic velocity, –	0.03	0.08	0.08	0.15	0.17

only when the pressure is at 100 kPa or 80 kPa. As the pressure decreases, discrepancy becomes notable; the experimental value at 20 kPa is 0.182 mm/s, which is 70% of the theory.

5. Discussion

It is quite interesting that the discrepancy is seen only for carbon dioxide. Also, previous work (Hoshino et al., 2010a) has shown satisfactory accordance between the prediction and the experiment for the air. As noted earlier, the theory contains four constants, C_M, C_T, C_S, and C_H, and the former two of these are calculated from accommodation coefficients α_m and α_t. These constants and coefficients have been determined empirically; different researchers have given different proposed values. Attempts should be made for finding suitable values to fit the prediction to these experimental results.

The first attempt is done by applying proposed values from references, which are shown in Table 2. The set of values noted as Case 1 is from the paper by Hoshino et al. (2010a), and those as Case 2 and 3 are both from the paper by Chang & Keh (2012). Fig. 7 shows predictions together with experimental results. The vertical axis represents the reduced thermophoretic velocity, which is a dimensionless parameter defined as follows:

$$V_{TR} \equiv \frac{V_T T_{F0}}{\upsilon \nabla T}, \tag{8}$$

where υ is the kinematic viscosity of the gas. This parameter is often used when making comparison between different conditions. Lines labeled as Prediction 1, 2, and 3 are those predicted from Eq. (1) by applying values of Case 1, 2, and 3, respectively. For both argon and nitrogen, the best fit to experimental results is Prediction 1, and then Prediction 3 follows; the velocity predicted from Case 3 is higher than the experiment at $Kn=0.25$ for both two gases, whereas that from Case 1 is within the error bar throughout all the measured range of Kn. For carbon dioxide, on the other hand, there is no line predicting satisfactorily the experimental result at $Kn=0.15$, though Prediction 3 seems to be better than Prediction 1. Prediction 2 can be omitted from the discussion since it obviously disagrees with the experiment for all gases.

Provisionally, Case 1 is chosen as the best among three cases; Case 3 is not good enough for high Kn for all tested gases in comparison to Case 1. Choosing Case 1 instead of Case 3 is also consistent with the previous work, in which experiments have been conducted in the air under the atmospheric pressure for particles of PMMA, alumina, and Zn (Suzuki et al., 2009b); as shown in Table 3, significant differences are seen between Case 3 and experimental results for alumina and Zn, whereas agreements are satisfactory for all particles with Case 1. In the theory, only the radius and the thermal conductivity are considered as particle-related parameters. It would be reasonable to assume that coefficients for CO_2 are different from those for other gases; Sharipov (2004) has reviewed related papers and summarized accommodation coefficients for various gases, in which CO_2 values are notably different from Ar and N_2.

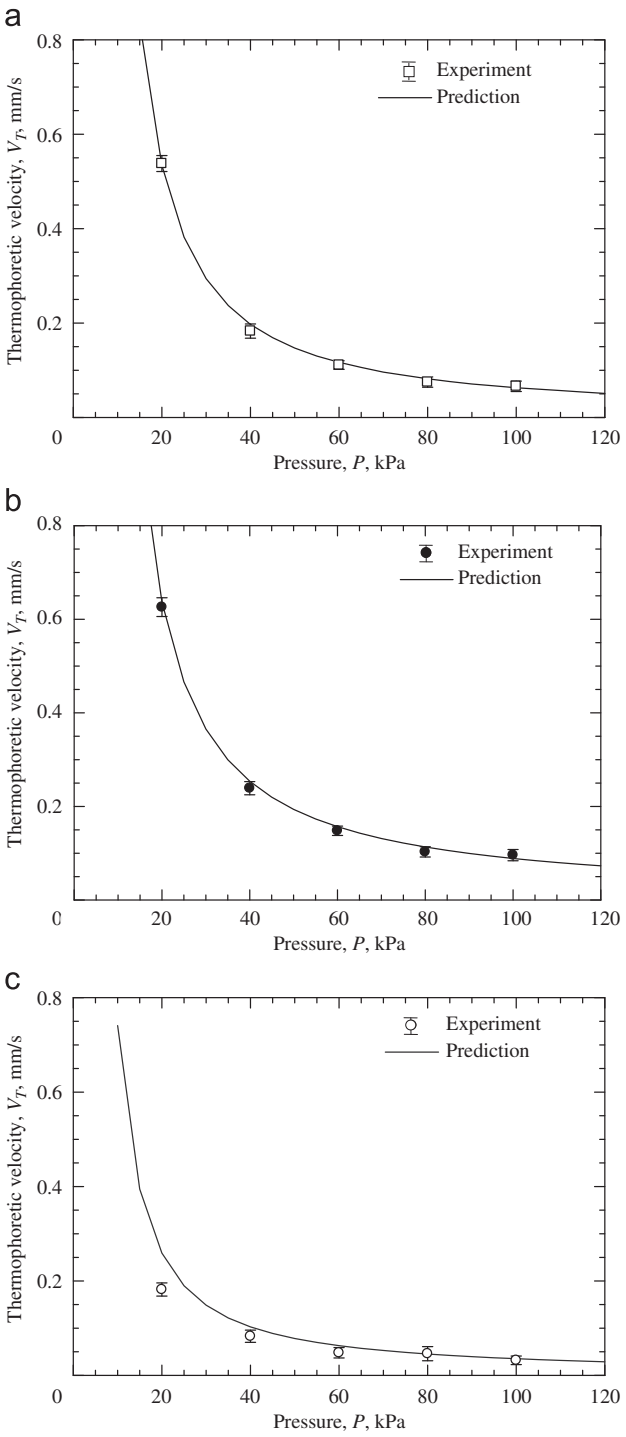

Fig. 6. Pressure dependence of thermophoretic velocity in each gas. Error bars represent the confidence interval (95%). Predictions are calculated under the assumption of C_M=1.000, C_T=1.875, C_S=0.750, and C_H=1.000: (a) argon, (b) nitrogen and (c) carbon dioxide.

Table 2
Constants for each case.

	C_M, –	C_T, –	C_S, –	C_H, –	α_m, –	α_t, –	References
Case 1	1.000	1.875	0.750	1.000	(1.000)[a]	(1.000)[a]	Hoshino et al. (2010a)
Case 2	1.140	2.180	1.170	1.000	(0.935)[a]	(0.925)[a]	Chang & Keh (2012)
Case 3	1.140	2.180	1.170	3.000	(0.935)[a]	(0.925)[a]	Chang & Keh (2012)

[a]Values in bracket are from Eqs. (4) and (5) (not directly given in the reference).

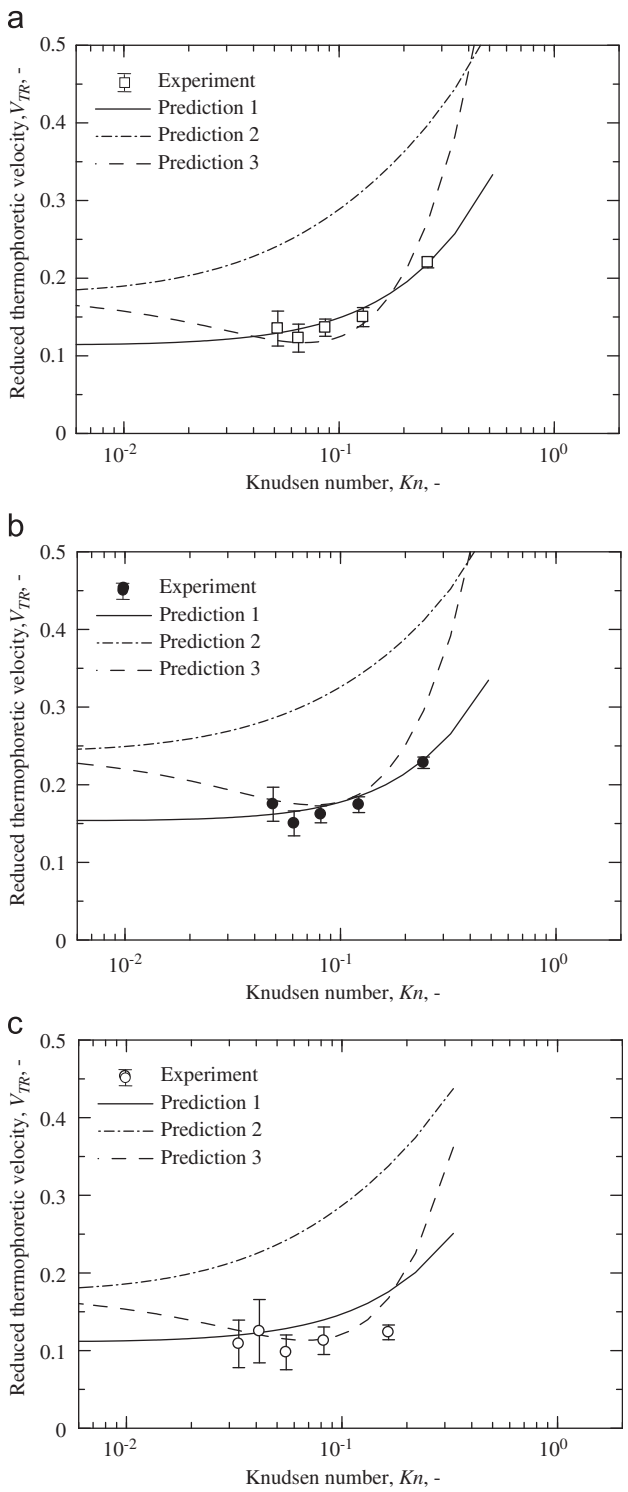

Fig. 7. Comparison between predictions and experiment in each gas Error bars represent the confidence interval (95%). Predictions are calculated using constants in Table 2: (a) argon, (b) nitrogen and (c) carbon dioxide.

The second attempt is done by changing the accommodation coefficients from Case 1 by means of the least square fit. The residue R representing the discrepancy between the experiment and the prediction is defined as follows:

$$R \equiv \sum_{j=1}^{n} (V_{ej} - V_{pj})^2, \ (j = 1,\ldots,n) \tag{9}$$

Table 3
Reduced thermophoretic velocity in air under atmospheric pressure.

Material	V_{TR}, –		Experiment[a]
	Prediction (Case 1)	Prediction (Case 3)	
PMMA	0.167	0.210	0.172 ± 0.011
Al_2O_3	0.037	−0.035	0.036 ± 0.008
Zn	0.049	−0.034	0.050 ± 0.010

[a] From Suzuki et al. (2009b).

Table 4
Estimated accommodation coefficients for carbon dioxide.

	α_m, –	α_t, –
Without limitation	1.193	1.307
With limitation	0.841	1.000

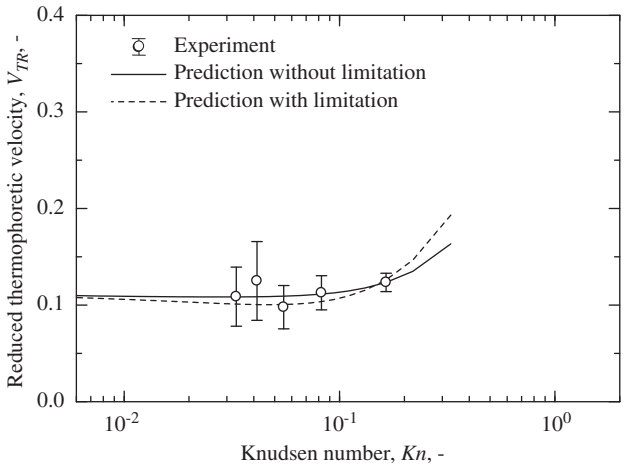

Fig. 8. Comparison of predictions for carbon dioxide Error bars represent the confidence interval (95%). The solid and the broken lines represent predictions calculated with the coefficients from least-square-fit "without limitation" and "with limitation", respectively.

where V_e, V_p, and n are thermophoretic velocities of the experiment and the prediction, and the number of the tested pressure conditions, respectively, and the subscript j refers to each tested condition. The values for C_S and C_H are unchanged from the Case 1, and those for C_M and C_T are calculated from Eqs. (4) and (5), respectively, with accommodation coefficients α_m and α_t determined such that the residue R becomes the lowest.

Table 4 shows the result of the least square fit for carbon dioxide. The best fit is attained with the coefficients noted as "without limitation" in the table. It should be noted that both values are clearly above unity, which is curious when interpreting the physical meaning of those values. Based on the kinetic theory, both those coefficients should lie between 0 and 1 (Brock, 1962; Kennard, 1938; Shen, 2010). The Cercignani-Lampis (CL) model provides a more physical description of the gas-surface interaction (Sharipov, 2003, 2004), which allows α_m to vary between 0 and 2 while α_t remains between 0 and 1. In this CL model, α_m can exceed unity when the surface is rough. Considering this, additional work is done for the fitting by applying the limitation of $0 \leq \alpha_t \leq 1$ and $0 \leq \alpha_m \leq 2$, the result of which is shown as "with limitation" in the table. In this case, R becomes the lowest when both the coefficients are bellow unity even α_m is allowed to exceed it.

Fig. 8 shows the comparison of predictions based on these values. It is seen that both predictions are in good agreement with the experiment within the range of the tested conditions. The difference between these two predictions is notable only under the condition of higher Knudsen number than the current work.

In order to interpret the different coefficients for the carbon dioxide, authors have found two different points of view from literatures so far; one is the molecular weight, and the other the diameter of a molecule. The former is based on the work by Gronych et al. (2004), who have conducted experiments to find out that the tangential momentum accommodation coefficient increases as the molecular weight of the gas decreases. This may be related to the influence of gas species. However, applying

this effect for the explanation of the present results would not be appropriate; the molecular weight of argon is closer to carbon dioxide rather than nitrogen, while the thermophoretic characteristic of the argon is much closer to the nitrogen rather than the carbon dioxide.

The latter is based on the work by Arya et al., (2003), who have conducted a molecular simulation for a wall-slip phenomenon in rarefied gases. According to their result, the tangential momentum accommodation coefficient decreases as the collision diameter of the molecule increases. Among the gases used in this work, carbon dioxide has a notably larger collision diameter; based on the rigid sphere model, the diameter of argon, nitrogen, and carbon dioxide are 3.659 Å, 3.784 Å, and 4.643 Å, respectively (Ivchenko et al., 2007). This can explain qualitatively the results in this work if the coefficients "with limitation" are adopted for the carbon dioxide and those at unity are adopted for other two gases. The thermal accommodation coefficient "with limitation" is also consistent with the work by Winkler et al. (2004), in which the coefficient α_t is reported to be approximately unity for water vapor, a polyatomic gas having a large collision diameter. The constants and coefficients, however, cannot be determined from the results in this work, since several combinations of those are possible to fit predictions to experimental results.

6. Conclusions

In this study, effects of gas species on the thermophoretic velocity are investigated, and following results are obtained:

1. Experimentally-obtained pressure dependence of the thermophoretic velocity for both argon and nitrogen are quantitatively in good agreement with the theory, while notable discrepancy is seen for carbon dioxide, if values for the constants C_M, C_T, C_S, and C_H to be 1.000, 1.875, 0.750, and 1.000 are applied to the theory.
2. Values of those empirical constants proposed in some references were applied to the theory and compared with experiments; none of those has reduced the notable deviation for the carbon dioxide at $Kn=0.15$.
3. The coefficients are calculated by means of the least square fit. The obtained values can be interpreted qualitatively by considering the effect of the molecular diameter on the tangential momentum accommodation coefficient. The proposed values of C_M, C_T, C_S, and C_H for carbon dioxide are 1.378, 1.875, 0.750, and 1.000, although further discussion will be required for the determination of the values.

Acknowledgement

A part of this work was supported by JSPS KAKENHI 24560225.

References

Arya, G., Chang, H.C., & Maginn, E.J. (2003). Molecular simulations of Knudsen wall-slip: effect of wall morphology. *Molecular Simulation*, *29*, 697–709.
Basset, A.B. (1961). *A Treatise on Hydrodynamics*, 2.
Brock, J.R. (1962). On the theory of thermal forces acting on aerosol. *Journal of Colloid Science*, *17*, 768–780.
Chang, Y.C., & Keh, H.J. (2012). Effects of thermal stress slip on thermophoresis and photophoresis. *Journal of Aerosol Science*, *50*, 1–10.
Davis, L.A., & Adair, T.W.I.I.I. (1975). Thermal force on a sphere. *Journal of Chemical Physics*, *62*, 2278–2285.
Derjaguin, B.V., & Yalamov, Yu. (1965). Theory of thermophoresis of large aerosol particles. *Journal of Colloid Science*, *20*, 555–570.
Dobashi, R., Kong, Z.W., Toda, A., Takahashi, N., Suzuki, M. & Hirano, T. (2000). Mechanism of smoke generation in a flickering pool flame. *Proceeding of the 6th International Symposium on Fire Safety Science*, 255–264.
Douglas, F.S. (1982). Energy and tangential momentum accommodation coefficients on gas covered tungsten. *Journal of Chemical Physics*, *76*, 3814–3818.
Fredlund, E. (1938). Absolute measurements of radiometric action in gases. *Philosophical Magazine*, *26*, 987–1000.
Gronych, T., Ulman, R., Peksa, L., & Repa, P. (2004). Measurements of the relative momentum accommodation coefficient for different gases with a viscosity vacuum gauge. *Vacuum*, *73*, 275–279.
Hoshino, A., Suzuki, M. & Masuda, W. (2010a). Numerical analysis on thermophoretic phenomenon in slip flow regime considering thermal stress effect. *The 21st International Symposium on Transport Phenomena*.
Hoshino, A., Suzuki, M., & Masuda, W., (2010b). Influence of particle size distribution on measurement accuracy of thermophoretic velocity. In: *Proceeding of the 48th Symposium (Japanese) on Combustion*, pp. 464–465.
Ivchenko, I.N., Loyalka, S.K., & Tompson, R.V., Jr. (2007). *Analytical Methods for Problems of Molecular Transport*. Springer: The Netherlands.
Jacobsen, S., & Brock, J.R. (1965). The thermal force on spherical sodium chloride aerosols. *Journal of Colloid Science*, *20*, 544–554.
Keng, E., & Orr, C. (1966). Thermal precipitation and particle conductivity. *Journal of Colloid and Interface Science*, *22*, 107–116.
Kennard, E.H. (1938). *Kinetic Theory*. McGraw-Hill: New York.
Kousaka, Y., Okuyama, K., Nishio, S., & Yoshida, T. (1976). Experimental study of thermophoresis of aerosol particles. *Journal of Chemical Engineering of Japan*, *9*, 147–150.
Li, W., & Davis, E.J. (1995a). Measurement of the thermophoretic force by electrodynamic levitation: microspheres in air. *Journal of Aerosol Science*, *26*, 1063–1083.
Li, W., & Davis, E.J. (1995b). The effects of gas and particle properties on thermophoresis. *Journal of Aerosol Science*, *26*, 1085–1099.
Lockerby, D.A., Reese, J.M., Emerson, D.R., & Barber, R.W. (2004). Velocity boundary condition at solid walls in rarefied gas calculations. *Physical Review E*, *70*, 017303–1-017303-4.
Prodi, F., Santachiara, G., Di Matteo, L., Vedernikov, A., Beresnev, S.A., & Chernyak, V.G. (2007). Measurements of thermophoretic velocities of aerosol particles in microgravity conditions in different carrier gases. *Journal of Aerosol Science*, *38*, 645–655.
Prodi, F., Santachiara, G., & Prodi, V. (1979). Measurements of thermophoretic velocities of aerosol particles in the transition region. *Journal of Aerosol Science*, *10*, 421–425.

Prodi, F., Santachiara, G., Travaini, S., Vedernikov, A., Dubois, F., Minetti, C., & Legros, J.C. (2006). Measurements of phoretic velocities of aerosol particles in microgravity conditions. *Atmospheric Research*, *82*, 183–189.
Rosenblatt, P., & La Mer, V.K. (1946). Motion of a particle in a temperature gradient; thermal repulsion as a radiometer phenomenon. *Physical Review*, *70*, 385–395.
Saxton, R.L., & Ranz, W.E. (1952). Thermal force on an aerosol particle in a temperature gradient. *Journal of Applied Physics*, *23*, 917–923.
Schadt, C.F., & Cadle, R.D. (1957). Thermal forces on aerosol particles in a thermal precipitator. *Journal of Colloid Science*, *12*, 356–362.
Schadt, C.F., & Cadle, R.D. (1961). Thermal forces on aerosol particles. *Journal of Physical Chemistry*, *65*, 1689–1694.
Sharipov, F. (2003). Application of the Cercignani-Lampis scattering kernel to calculations of rarefied gas flows. III. Poiseuille flow and thermal creep through a long tube. *European Journal of Mechanics B/Fluids*, *22*, 145–154.
Sharipov, F. (2004). Data on the velocity slip and temperature jump coefficients. *Proceeding of Euro SimE*, 243-249.
Shen, C. (2010). *Rarefied Gas Dynamic: Fundamentals, Simulation, and Micro Flows*. Springer: Germany.
Suzuki, M., Maruko, K., Iwahara, K. & Masuda, W. (2009a). Accurate measurement of thermophoretic velocity under high temperature gradient. 6th *International Symposium on Scale Modelling (ISSM6)*, 1.12.1–1.12.8.
Suzuki, S. & Dobashi, R. (2007). Thermophoretic effect on soot particle behavior influence of particle morphology. 21st ICDERS, 239.
Suzuki, T., Suzuki, M. & Masuda, W. (2009b). Effect of water vapor to thermophoresis phenomenon. *Proceeding of the 47th Symposium (Japanese) on Combustion*, 448–449.
Talbot, L., Cheng, R.K., Schefer, R.W., & Willis, D.R. (1980). Thermophoresis of particles in a heated boundary layer. *Journal of Fluid Mechanics*, *101*, 737–758.
Thomas, L.B., & Lord, R.G. (1974). Comparative measurements of tangential momentum and thermal accommodations on polished and on roughened steel spheres. *International Symposium on Rarefied Gas Dynamics*, *8*, 405–412.
Toda, A., Ohi, Y., Dobashi, R., Hirano, T., & Sakuraya, T. (1996). Accurate measurement of thermophoretic effect in microgravity. *Journal of Chemical Physics*, *105*, 7083–7087.
Toda, A., Ohnishi, H., Dobashi, R., Hirano, T., & Sakuraya, T. (1998). Experimental study on the relation between thermophoresis and size of aerosol particles. *International Journal of Heat and Mass Transfer*, *41*, 2710–2713.
Tong, N.T. (1975). Experiments on photophoresis and thermophoresis. *Journal of Colloid and Interface Science*, *51*, 143–151.
Winkler, P.M., Vrtala, A., Wagner, P.E., Kulmala, M., Lehtinen, K.E.J., & Vesala, T. (2004). Mass and thermal accommodation during gas-liquid condensation of water. *Physical Review Letters*, *93*, 075701–1-075701-4.
Yuasa, Y., Sasaki, H. & Tsukamoto, T. (2011). Particle size distribution of particulate matter exhausted from four stroke marine diesel engine. *Proceeding of the 49th Symposium (Japanese) on Combustion*, 310–311.
Zheng, F., & Davis, E.J. (2001). Thermophoretic force measurements of aggregates of micro-spheres. *Journal of Aerosol Science*, *32*, 1421–1435.